J. Fluid Mech. (1989), *vol.* 208, *pp.* 25–43
Printed in Great Britain

Loss of frequency response along sampling tubes for the measurements of gaseous composition at high temperature and pressures

By RONALD SMITH

Department of Applied Mathematics and Theoretical Physics, University of Cambridge, Silver Street, Cambridge CB3 9EW, UK

(Received 24 June 1988 and in revised form 21 April 1989)

Measurements of the rapidly changing gaseous composition in engines at low speed can be made via narrow tubes which convey the gases to monitoring equipment in a less hostile environment. This paper quantifies the extent to which the tube smooths out any changes in concentration. Exact (and approximate) formulae are derived for the temporal variance as weighted double (and single) integrals of the steady flow properties along the tube. Such is the non-uniformity that typically the region near the engine contributes 100 times as much to the spreading as does the region near the monitoring equipment. The advantages of keeping the sampling tubes short and heated are made explicit.

1. Introduction

In any combustion chamber, the initiation and progress of the reaction depends in part on the local value of the fuel to air ratio. In some situations, for example internal combustion engines, there is evidence (Johnson 1979) that it is the variations from cycle to cycle in the fuel concentration that are responsible for the well-known and undesirable fluctuations in cyclic work output, particularly at low engine speeds.

In a recent paper, Collings (1988) reported a new technique for continuous sampling and measurement of the fuel–air mixture from a gasoline engine, using a very fine capillary tube inserted through the sparking plug. The sample was driven by the large pressure differences between the engine cylinder and the detection apparatus. At low engine speeds the flow could be regarded as being quasi-steady. Longitudinal mixing along the capillary tube limits the frequency response of the measurements.

The purpose of the present paper is to investigate this loss of frequency response, with the flow regarded as being steady. Because of the marked non-uniformity (of temperature, pressure, density...) along the capillary, conventional calculations of dispersion (Taylor 1953; Philip 1963*a*, *b*, *c*) are inapplicable. In the context of dispersion in rivers, Smith (1984) showed that longitudinal non-uniformity could be accounted for by taking moments with respect to time of the concentration distribution (Tsai & Holley 1978, 1980). Here we shall follow an equivalent pattern of calculations, but formulated in terms of the Laplace transform of the concentration. The main outcome is an explicit formula (13.5) for the sharpness of the response. The formula reveals that it is desirable to make the sampling tube as short and as hot as is compatible with the operation of the measuring device.

Curiously, the shear dispersion coefficient typically increases by a factor of 10 from the engine to the monitoring equipment. Yet, the contribution per unit length of

sampling tube to the temporal smearing decreases by a factor of 100. So simple estimates of the spreading based upon averaged flow properties could be seriously in error.

2. Advection–diffusion equation

For a narrow capillary, any radial velocity will be negligible except within a few diameters of the entry and of the exit. Vorticity within the engine can give rise to swirling flow within the initial reaches of the capillary tube. This can help to eliminate any angular variations in velocity or concentration (Rhines & Young 1983). Provided that any bends are very gentle relative to the internal diameter, swirl does not have much effect upon longitudinal dispersion in tubes (Erdogan & Chatwin 1967). So, as the starting point of our mathematical analysis, we shall assume that there is no radial flow and there is no angular variation in velocity or concentration.

If the flow is reasonably fast, then the Péclet number will be moderately large, and advection will greatly dominate longitudinal molecular diffusion (Taylor 1953). Thus, in calculating the concentration $c(x, r, t)$ of any one gaseous species, we need only account for molecular diffusion across the flow:

$$\partial_t c + u\partial_x c - \frac{\kappa}{a^2 r}\partial_r(r\partial_r c) = 0. \tag{2.1}$$

In this equation t is time, x the longitudinal coordinate, $a(x)$ the capillary radius, r the dimensionless radial coordinate, $u(x, r)$ the longitudinal velocity, and $\kappa(x)$ the molecular diffusivity. Chemical reactions within the capillary have been ignored. If the material of the capillary tube is impermeable to the particular chemical species, then

$$\kappa\partial_r c = 0 \quad \text{on} \quad r = 1. \tag{2.2}$$

The conservation of mass for a steady flow can be written

$$\partial_x(\rho a^2 u) = 0 \tag{2.3}$$

where ρ is the density. For simplicity we shall neglect any radial variation of ρ (just as we have already done for the molecular diffusivity κ). The longitudinal dependence of the coefficients ρ, u, κ stems from the compressibility and the considerable pressure differences between the interior of the engine and the external gas measurement equipment. In neglecting the time-dependence of ρ it is implicit that the transit time along the sampling tube is short compared with the rate of firing of the engine.

3. Laplace transforms

We suppose that at some (possibly remote) starting time t_0 the concentration was identically zero throughout the capillary tube. Relative to that time, we define the Laplace transform

$$\hat{c}(x, r, p) = \int_0^\infty \mathrm{e}^{-p\tau} c(x, r, t_0 + \tau)\,\mathrm{d}\tau. \tag{3.1}$$

The transform of the advection–diffusion equation (2.1) is

$$p\hat{c} + u\partial_x \hat{c} - \frac{\kappa}{a^2 r}\partial_r(r\partial_r \hat{c}) = 0, \tag{3.2a}$$

with $$\kappa \partial_r \hat{c} = 0 \quad \text{on} \quad r = 1, \tag{3.2b}$$

and $$\hat{c} = \hat{c}_I(p) \quad \text{at} \quad x = 0. \tag{3.2c}$$

Here $\hat{c}_I$ is the Laplace transform of the inlet concentration, which is assumed to be uniform across the capillary.

If the flow properties were uniform with respect to x, then (3.2*a–c*) could be solved by separation of variables. Philip (1963*a*, *b*, *c*) gives the mathematical details, using Fourier rather than Laplace transforms. The next section gives the counterpart to separation of variables in the non-uniform case.

4. Eigenfunction expansion

To solve (3.2*a–c*), we formally introduce eigenmodes going with and against the flow (Smith 1983, §7):

$$\frac{\kappa}{a^2 r} \partial_r (r \partial_r \Psi_n^{(\pm)}) + \lambda_n u \Psi_n^{(\pm)} - p \Psi_n^{(\pm)} = \pm u \partial_x \Psi_n^{(\pm)}, \tag{4.1a}$$

with $$\kappa \partial_r \Psi_n^{(\pm)} = 0 \quad \text{on} \quad r = 1, \tag{4.1b}$$

$$\overline{u \Psi_n^{(+)} \Psi_n^{(-)}} = \bar{u}, \quad \overline{u \Psi_n^{(+)} \Psi_j^{(-)}} = 0 \quad (n \neq j), \tag{4.1c}$$

$$\overline{u \Psi_n^{(+)} \partial_x \Psi_n^{(-)}} = \overline{u \Psi_n^{(-)} \partial_x \Psi_n^{(+)}} = 0, \tag{4.1d}$$

$$\Psi_n^{(+)} = \Psi_n^{(-)} \quad \text{at} \quad x = 0, L. \tag{4.1e}$$

The overbars denote cross-sectional average values

$$\bar{f} = 2 \int_0^1 f(r) r \, \mathrm{d}r \tag{4.2}$$

The conditions (4.1*d*, *e*) serve to minimize the x-dependence. Thus, in the conventional case with u, κ independent of x, the adjoint modes $\Psi_n^{(+)}(x, r, p)$, $\Psi^{(-)}(x, r, p)$ become the same as each other and independent of x.

The integral identity

$$\lambda_n \bar{u} = \frac{\kappa}{a^2} \overline{\partial_r \Psi_n^{(+)} \partial_r \Psi_n^{(-)}} + p \overline{\Psi_n^{(+)} \Psi_n^{(-)}} \tag{4.3}$$

reveals that λ_n increases with the transform parameter p, and for increasingly oscillatory modes. Conventionally the labelling of the modes is such that

$$\lambda_0 < \lambda_1 < \lambda_2 < \ldots. \tag{4.4}$$

When $p = 0$ the lowest mode is non-decaying and uniform across the flow

$$\lambda_0 = 0, \quad \Psi_0^{(+)} = \Psi_0^{(-)} = 0 \quad \text{for} \quad p = 0. \tag{4.5a, b}$$

The formal solution of (3.2*a–c*) can be written

$$\hat{c} = \hat{c}_I \sum_{n=0}^{\infty} \overline{\left(\frac{u}{\bar{u}}\right) \Psi_n^{(-)}}(0, p) \, \Psi_n^{(+)}(x, r, p) \exp\left(- \int_0^x \lambda_n(x', p) \, \mathrm{d}x' \right). \tag{4.6}$$

Hence, if the capillary tube is reasonably long (compared with a mixing length for diffusion across the flow), we can neglect all but the $n = 0$ mode. Likewise, the more rapid attenuation of the large-p components, means that we should focus our attention upon small values of the transform parameter p.

5. Taylor series for small p

To solve equations (4.1a–e) for the slowest-decaying modes $\Psi_0^{(+)}$ and $\Psi_0^{(-)}$, we employ series expansions for small p:

$$\Psi_0^{(\pm)} = 1 - pG^{(\pm)}(x,r) + \ldots, \tag{5.1a}$$

$$\lambda_0 = \frac{p}{\bar{u}} - \frac{p^2\kappa}{\bar{u}a^2}\overline{\partial_r G^{(+)}\,\partial_r G^{(-)}} + \ldots. \tag{5.1b}$$

The time-lag functions $G^{(+)}$, $G^{(-)}$ satisfy the equations (Smith 1984, equations (4.8), (4.2)):

$$\pm u\partial_x G^{(\pm)} - \frac{\kappa}{a^2 r}\partial_r(r\partial_r G^{(\pm)}) = 1 - \frac{u}{\bar{u}}, \tag{5.2a}$$

with

$$\kappa\partial_r G^{(\pm)} = 0 \quad \text{on} \quad r = 1, \tag{5.2b}$$

$$\overline{uG^{(\pm)}} = 0, \tag{5.2c}$$

$$G^{(+)} = G^{(-)} \quad \text{at} \quad x = 0, L. \tag{5.2d}$$

Although we shall not extend the full calculations to order p^2, the end boundary condition (4.1e) together with the normalization (4.1c), permits us to deduce that

$$\overline{u\Psi^{(\pm)}} = \bar{u} - \tfrac{1}{2}p^2\overline{uG^{(+)}G^{(-)}} + \ldots \quad \text{at} \quad x = 0, L. \tag{5.3}$$

So, at $x = L$, the flux-weighted form of the asymptote (4.6) can be written

$$\overline{\left(\frac{u}{\bar{u}}\right)}\hat{c} = \hat{c}_1\left[1 - \tfrac{1}{2}p^2\left(\left.\frac{\overline{uG^2}}{\bar{u}}\right|_0 + \left.\frac{\overline{uG^2}}{\bar{u}}\right|_L\right) + \ldots\right]\exp(-\phi(L,p)), \tag{5.4a}$$

where

$$\phi = p\int_0^L \frac{\mathrm{d}x}{\bar{u}} - p^2\int_0^L \frac{\kappa}{\bar{u}a^2}\overline{\partial_r G^{(+)}\,\partial_r G^{(-)}}\,\mathrm{d}x' + \ldots. \tag{5.4b}$$

Hence, at the exit we can achieve second-order accuracy with only the first-order solution.

6. A comparison problem

To determine the complete response at the exit $x = L$, we should need to know $\hat{c}$ to arbitrary accuracy in p. This is far beyond the scope of the present calculations. Instead, we shall extend the two-term expansion (5.4b) by comparison with the work of Taylor (1953).

For uniform flows, Taylor (1953) derived a constant-coefficient model of the shear dispersion process

$$\partial_t C + U\partial_x C - D\partial_x^2 C = 0, \tag{6.1a}$$

with

$$C = C_{\mathrm{I}} \quad \text{at} \quad X = 0. \tag{6.1b}$$

The use of capital letters is to emphasize the difference between this uniform situation and the non-uniform situation studied in the rest of the present paper.

The Laplace transform solution is

$$\hat{C} = \hat{C}_{\mathrm{I}}\exp(-\Phi), \tag{6.2a}$$

where

$$\Phi = \frac{XU}{2D}\left[\left(1 + 4\frac{pD}{U^2}\right)^{\frac{1}{2}} - 1\right] = \frac{pX}{U} - \frac{p^2XD}{U^3} + \ldots. \tag{6.2b}$$

From the tables of Laplace transforms given by Carslaw & Jaeger (1959, Appendix 6), we can obtain the inversion

$$C(X,t) = \int_0^\infty I(X,\tau)\, C_{\mathrm{I}}(t-\tau)\,\mathrm{d}\tau, \tag{6.3a}$$

$$I(X,\tau) = \frac{X}{2(\pi D)^{\frac{1}{2}}\tau^{\frac{3}{2}}}\exp\left(-\frac{(X-U\tau)^2}{4D\tau}\right). \tag{6.3b}$$

7. Linking the approximate and idealized solutions

As we should expect, there is a strong resemblance between the formulae (5.4), (6.2) for the Laplace transforms of the concentrations $\hat{c}$, $\hat{C}$. To make the connection quantitative, we define the transit time T, and a temporal variance contribution σ^2:

$$T(L) = \int_0^L \frac{\mathrm{d}x}{\bar{u}}, \tag{7.1a}$$

$$\sigma^2(L) = 2\int_0^L \frac{\kappa}{\bar{u}a^2}\,\overline{\partial_r G^{(+)}\,\partial_r G^{(-)}}\,\mathrm{d}x'. \tag{7.1b}$$

Instead of the truncated series (5.4*b*) for the decay exponent ϕ, we pose the formula

$$\phi(L,p) = \frac{T^2}{\sigma^2}\left[\left(1+\frac{2p\sigma^2}{T}\right)^{\frac{1}{2}}-1\right]. \tag{7.2}$$

To account for the end corrections in the formula (5.4*a*), we define the deficit variance Δ^2:

$$\Delta^2 = \left.\frac{\overline{uG^2}}{\bar{u}}\right|_0 + \left.\frac{\overline{uG^2}}{\bar{u}}\right|_L. \tag{7.3}$$

The quotient σ^2/Δ^2 gives an estimate of the number of mixing lengths between the engine and the detection equipment, so should be large.

An *ad hoc* extension of the asymptote (5.4) which retains the order-p^2 accuracy and has an explicit inversion is

$$\overline{\left(\frac{u}{\bar{u}}\right)\hat{c}} = \hat{c}_{\mathrm{I}}\left[1-\frac{\Delta^2 T^2\{(1+2p\sigma^2/T)^{\frac{1}{2}}-1\}^2}{2\sigma^4(1+2p\sigma^2/T)}\right]\exp(-\phi). \tag{7.4}$$

The Laplace inversion is

$$\overline{\left(\frac{u}{\bar{u}}\right)c} = \int_0^\infty J(L,\tau)\, c_{\mathrm{I}}(T-\tau)\,\mathrm{d}\tau, \tag{7.5a}$$

with

$$\begin{aligned} J(L,\tau) = {} & \left[1-\frac{\Delta^2T^2}{2\sigma^4}\right]\frac{1}{(2\pi\sigma^2)^{\frac{1}{2}}}\left(\frac{T}{\tau}\right)^{\frac{3}{2}}\exp\left(-\frac{(T-\tau)^2T}{2\sigma^2\tau}\right) \\ & +\frac{\Delta^2T^2}{\sigma^4}\frac{1}{(2\pi\sigma^2)^{\frac{1}{2}}}\left(\frac{T}{\tau}\right)^{\frac{1}{2}}\exp\left(-\frac{(T-\tau)^2T}{2\sigma^2\tau}\right) \\ & -\frac{\Delta^2T^2}{2\sigma^4}\left(\frac{T}{\sigma^2}\right)\exp\left(\frac{T^2-\frac{1}{2}\tau T}{\sigma^2}\right)\mathrm{erfc}\left(\frac{T^{\frac{3}{2}}}{(2\sigma^2\tau)^{\frac{1}{2}}}\right). \end{aligned} \tag{7.5b}$$

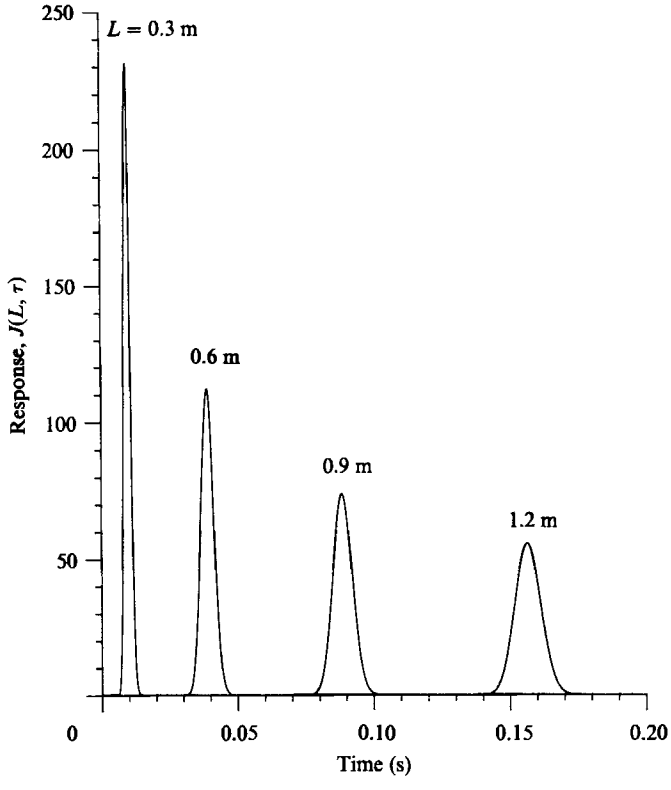

FIGURE 1. Response function for tubes of different lengths. For lighter molecular weight fuels the response is even sharper.

Formulae (12.12a), (13.5), (13.10) are derived later for T, σ^2 and Δ^2. As an illustrative example, we specify the isothermal flow conditions

$$\left.\begin{aligned} \text{Internal pressure} = 10 \text{ bar}, \quad \text{External pressure} = 1 \text{ bar}, \\ \text{Capillary radius} = 0.05 \text{ mm}, \quad \text{Absolute temperature} = 500 \text{ K}. \end{aligned}\right\} \tag{7.6}$$

(All subsequent numerical examples will correspond to this particular specification and with a diffusivity appropriate to a fixed chemical component of the hydrocarbon fuel.) Figure 1 shows the predicted response function J for different tube lengths L measured in metres. For short tubes there is remarkably little temporal smearing, though the response becomes less sharp for longer sampling lines.

8. Time-lag functions

The velocity profile adjusts more rapidly than the time-lag functions to any changes in conditions along the capillary. In part (a factor of 1.5^2), this is due to the much greater stiffness of a no-slip boundary condition (zero value) as compared with a zero-flux condition. However, there is also a disparity between the laminar viscosity ν and the molecular diffusivity κ, particularly for higher molecular weight constituents such as hydrocarbons (a further factor of 6.6). Thus, we shall model the velocity profile as being in the equilibrium form

$$u = 2\,\bar{u}(1-r^2). \tag{8.1}$$

With this parabolic velocity profile, the e-folding length for the time-lag functions to respond to any changes is approximately

$$\frac{a^2\bar{u}}{16\kappa}. \tag{8.2}$$

For example, if

$$a = 0.05\,\text{mm},\ \bar{u} = 200\ \text{ms}^{-1},\ \kappa = 5\ \text{mm}^2\,\text{s}^{-1}, \tag{8.3}$$

then the e-folding length would be approximately 6.25 mm. The magnitude of the pressure drop between the inside of an operational engine and the external monitoring equipment is such that there can be significant changes in flow properties even on distances as short as 6.25 mm. Thus, we need to take due account of the x-dependence of the time-lag functions $G^{(+)}$ and $G^{(-)}$.

We introduce an intrinsic downstream coordinate

$$\xi = \int_0^x \frac{\kappa}{a^2\bar{u}}\mathrm{d}x', \quad l = \int_0^L \frac{\kappa}{a^2\bar{u}}\mathrm{d}x'. \tag{8.4a,b}$$

In terms of ξ the local e-folding distance is of order $\frac{1}{16}$. The field equation (5.2a) for the time-lag functions becomes

$$\pm\frac{u}{\bar{u}}\partial_\xi G^{(\pm)} - \frac{1}{r}\partial_r(r\partial_r G^{(\pm)}) = \frac{a^2}{\kappa}\left(1-\frac{u}{\bar{u}}\right), \tag{8.5}$$

If, as in (8.1), the velocity profile remains self-similar, then the longitudinal non-uniformity is relegated to the right-hand-side forcing.

To solve (8.5), we can employ conventional self-adjoint modes (neither x-dependence, nor p-dependence):

$$\frac{\mathrm{d}}{\mathrm{d}r}\left(r\frac{\mathrm{d}\phi_n}{\mathrm{d}r}\right) + \lambda_n r\left(\frac{u}{\bar{u}}\right)\phi_n = 0, \tag{8.6a}$$

$$\frac{\mathrm{d}\phi_n}{\mathrm{d}r} = 0 \quad \text{on} \quad r = 1, \tag{8.6b}$$

$$\overline{u\phi_n^2} = \bar{u}, \quad \overline{u\phi_n\phi_j} = 0 \quad (n \neq j). \tag{8.6c}$$

For Poiseuille flow it is not possible to express the modes in closed form. However, a convenient single-mode approximation is

$$\lambda^* = 16, \quad \phi^* = \sqrt{3}\{-1+4r^2-2r^4\}, \quad \overline{\phi^*} = \frac{1}{\sqrt{3}}. \tag{8.7a–c}$$

The construction of such approximations is discussed in Appendix A.

We pose eigenfunction expansions

$$G^{(\pm)}(\xi, r) = \sum_{n=1}^{\infty} G_n^{(\pm)}(\xi)\,\phi_n(r), \tag{8.8}$$

The normalization (5.2c) precludes any contributions from the zero mode $\phi_0 = 1$. The coefficients $G_n^{(\pm)}(\xi)$ satisfy ordinary differential equations

$$\pm\frac{\mathrm{d}G_n^{(\pm)}}{\mathrm{d}\xi} + \lambda_n G_n^{(\pm)} = \frac{a^2}{\kappa}\bar{\phi}_n, \tag{8.9a}$$

$$G_n^{(+)} = G_n^{(-)} \quad \text{at} \quad \xi = 0, l. \tag{8.9b}$$

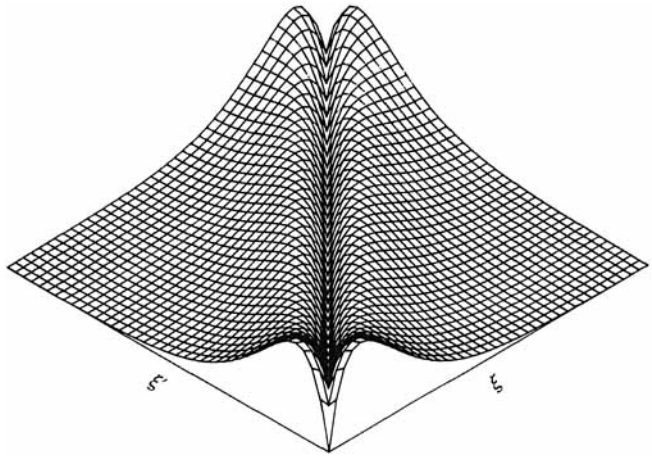

FIGURE 2. The weight function $W(\xi, \xi')$ for the double-integral formula for the main contribution $\sigma^2(L)$ to the temporal variance.

The solutions for the coefficients $G_n^{(\pm)}$ are

$$G_n^{(\pm)} = \frac{\exp(\pm\lambda_n(l-\xi))\,\bar{\phi}_n}{\sinh\lambda_n l}\int_0^{\xi}\frac{a^2}{\kappa}\cosh\lambda_n\xi'\,\mathrm{d}\xi' + \frac{\exp(\mp\lambda_n\xi)\,\bar{\phi}_n}{\sinh\lambda_n l}\int_{\xi}^{l}\frac{a^2}{\kappa}\cosh(\lambda_n(l-\xi'))\,\mathrm{d}\xi'. \quad (8.10)$$

For $G_n^{(+)}$ greatest weight is given to an upstream region of size $1/\lambda_n$, while for $G_n^{(-)}$ it is the downstream values of a^2/κ that contribute most strongly.

9. Formula for the temporal variance

In terms of the eigenfunction expansions (8.8*a*,*b*), the definition (7.1*b*) for σ^2 becomes

$$\sigma^2 = 2\sum_{n=1}^{\infty}\int_0^l \lambda_n G_n^{(+)}G_n^{(-)}\,\mathrm{d}\xi. \quad (9.1)$$

Substituting for $G_n^{(\pm)}$ from the integral expressions (8.6), we find that σ^2 can be related to a double integral of a^2/κ along the capillary tube:

$$\sigma^2(L) = 2\int_0^l\int_0^l \frac{a^2}{\kappa}\bigg|_{\xi}\frac{a^2}{\kappa}\bigg|_{\xi'} W(\xi,\xi')\,\mathrm{d}\xi\,\mathrm{d}\xi'. \quad (9.2)$$

In terms of the eigenmodes, the weight function $W(\xi, \xi')$ has the series representation

$$W(\xi,\xi') = \sum_{n=1}^{\infty}\frac{(\bar{\phi}_n)^2}{\sinh^2\lambda_n l}\{\lambda_n(l-\xi')\cosh\lambda_n\xi\cosh\lambda_n\xi' + \lambda_n(\xi'-\xi)\cosh\lambda_n\xi\cosh\lambda_n(l-\xi')\cosh\lambda_n l + \lambda_n\xi\cosh\lambda_n(l-\xi)\cosh\lambda_n(l-\xi')\} \quad \text{for} \quad \xi<\xi'. \quad (9.3)$$

The expression for $\xi' < \xi$ requires the interchanging of ξ and ξ'.

Figure 2 gives a perspective view of the one-mode weight function for the case

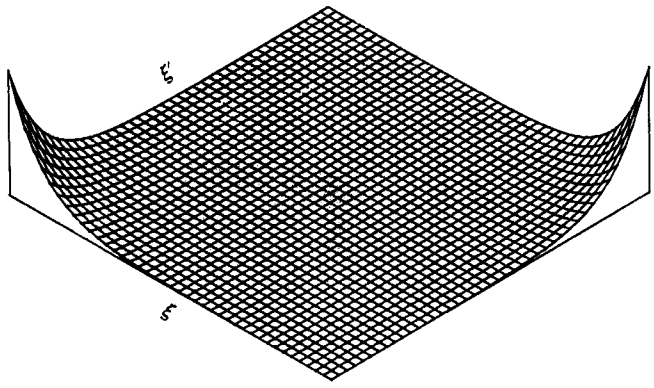

FIGURE 3. The weight function $V(\xi,\xi')$ for the double-integral formula for the (end correction) deficit variance Δ^2. (Note that the view is at right angles to that in the previous figure.)

$\lambda^* l = 10$. The dip in values along the diagonal $\xi = \xi'$ shows that the shear dispersion process is not quite local. It is the correlation of a^2/κ over distances of the order of one mixing length that determines the dispersion.

An incidental property of W that relates to the construction (8.3) of the one-mode approximation (λ^*, ϕ^*) is

$$\int_0^l W(\xi,\xi')\,\mathrm{d}\xi' = \sum_{n=1}^{\infty} \frac{(\bar{\phi}_n)^2}{\lambda_n} = \frac{(\bar{\phi}^*)^2}{\lambda^*} \quad \text{for} \quad 0 < \xi < l. \tag{9.4}$$

Reverting to the use of the conventional x-coordinate, the double-integral formula (9.2) for the principal contribution σ^2 to the temporal variance becomes

$$\sigma^2(L) = 2\int_0^L \int_0^L W(x,x') \frac{\mathrm{d}x\,\mathrm{d}x'}{\bar{u}(x)\,\bar{u}(x')}. \tag{9.5}$$

The terminology 'slowness' is sometimes used to describe the reciprocal of a velocity. Hence the result (9.5) gives the amount of temporal spreading as a weighted double integral over the length of the capillary of the slowness. Equivalently, the importance as regards dispersion of a region of the flow is a weighted double integral of the amount of time that the contaminant spends in each part of the flow. In particular, it is the slower high-pressure flow near the engine that dominates the total spreading.

10. Formula for the deficit variance

The initial inefficiency of the shear-dispersion process extremely close to the entry $x = 0$, and the lack of time/distance to respond to the conditions near the exit $x = L$, are accounted for in the deficit variance

$$\Delta^2 = \sum_{n=1}^{\infty} (G_n^2|_0 + G_n^2|_L). \tag{10.1}$$

The double-integral formulation is

$$\Delta^2 = 2\int_0^L \int_0^L \frac{a^2}{\kappa}\left|\frac{a^2}{\kappa}\right|_{\xi} V(\xi,\xi')\,\mathrm{d}\xi\,\mathrm{d}\xi', \tag{10.2}$$

where

$$V(\xi,\xi') = \sum_{n-1}^{\infty} \frac{(\bar{\phi}_n)^2}{2\sinh^2\lambda_n l}\{\cosh\lambda_n(l-\xi)\cosh\lambda_n(l-\xi') + \cosh\lambda_n\xi\cosh\lambda_n\xi'\}. \tag{10.3}$$

Figure 3 gives a perspective view of the one-mode weight function in the case $\lambda^* l = 10$. The rapid decay away from the end points is consistent with the interpretation of Δ^2 as an end correction to the total temporal variance $\sigma^2 - \Delta^2$.

An incidental property of V that relates to the construction (8.3) of the one-mode approximation is

$$\int_0^L \int_0^L V(\xi, \xi')\, \mathrm{d}\xi\, \mathrm{d}\xi' = \sum_{n=1}^{\infty} \frac{(\bar{\phi}_n)^2}{\lambda_n^2} = \frac{(\bar{\phi}_n^*)^2}{\lambda_n^{*2}}. \tag{10.4}$$

11. Exponentially varying flows

The strongly diagonal form of the weight function $W(\xi, \xi')$ as evidenced in figure 2, is strongly suggestive that for gradually varying flows the integral is effectively one-dimensional. Thus, we replace ξ, ξ' by the diagonal coordinates χ, η:

$$\chi = \tfrac{1}{2}(\xi + \xi'), \quad \eta = \tfrac{1}{2}(\xi - \xi'), \quad \xi = \chi + \eta, \quad \xi' = \chi - \eta. \tag{11.1a–d}$$

The double integral (9.2) for the principal contribution σ^2 to the temporal variance becomes

$$\sigma^2(L) = 4 \int_0^{l/2} \mathrm{d}\chi \int_{-\chi}^{\chi} \mathrm{d}\eta \frac{a^2}{\kappa}\bigg|_{\chi+\eta} \frac{a^2}{\kappa}\bigg|_{\chi-\eta} W(\chi, \eta) + 4 \int_{l/2}^{l} \mathrm{d}\chi \int_{-(l-\chi)}^{l-\chi} \mathrm{d}\eta \frac{a^2}{\kappa}\bigg|_{\chi+\eta} \frac{a^2}{\kappa}\bigg|_{\chi-\eta} W(\chi, \eta). \tag{11.2}$$

Assuming that a^2/κ varies exponentially over distances of the order of one mixing length, we pose the approximation

$$\frac{a^2}{\kappa}\bigg|_{\chi+\eta} \frac{a^2}{\kappa}\bigg|_{\chi-\eta} = \frac{a^4}{\kappa^2}\bigg|_{\chi}. \tag{11.3}$$

Hence, the η-integrations only involve W:

$$\tilde{W}(\chi) = 2 \int_{-\chi}^{\chi} W(\chi, \eta)\, \mathrm{d}\eta \quad \text{for} \quad \chi < \tfrac{1}{2} l, \tag{11.4a}$$

$$\tilde{W}(\chi) = 2 \int_{-(l-\chi)}^{l-\chi} W(\chi, \eta)\, \mathrm{d}\eta \quad \text{for} \quad \chi > \tfrac{1}{2} l. \tag{11.4b}$$

The resulting one-dimensional integral representation for σ^2 is

$$\sigma^2(L) = 2 \int_0^l \frac{a^4}{\kappa^2} \tilde{W}(\chi)\, \mathrm{d}\chi. \tag{11.5}$$

Evaluating the necessary integrals, we obtain

$$\begin{aligned} \tilde{W}(\chi) = \left(\sum_{n=1}^{\infty} \frac{(\bar{\phi}_n)^2}{\lambda_n} \right) - \sum_{n=1}^{\infty} \frac{(\bar{\phi}_n)^2}{\lambda_n \sinh^2 \lambda_n l} \{ & \cosh \lambda_n l \cosh \lambda_n (l - 2Z) - \cosh 2\lambda_n Z \\ & + 2\lambda_n Z \cosh \lambda_n l \sinh \lambda_n (l - 2Z) - \lambda_n (l - 2Z) \sinh 2\lambda_n Z \\ & - \lambda_n^2 Z^2 \cosh \lambda_n (l - 2Z) \cosh \lambda_n l - \lambda_n^2 Z^2 \cosh 2\lambda_n (l - Z) \\ & - \lambda_n^2 Z (2l - 3Z) \cosh 2\lambda_n Z \}, \end{aligned} \tag{11.6a}$$

where

$$Z = \min(\chi, l - \chi). \tag{11.6b}$$

The corresponding expression for $\tilde{V}(\chi)$ is

$$\tilde{V}(\chi) = \sum_{n=1}^{\infty} \frac{(\bar{\phi}_n)^2}{2\lambda_n \sinh^2 \lambda_n l} \{ \lambda_n Z \cosh 2\lambda_n (l - Z) + \sinh 2\lambda_n Z + \lambda_n Z \cosh 2\lambda_n Z \}. \tag{11.7}$$

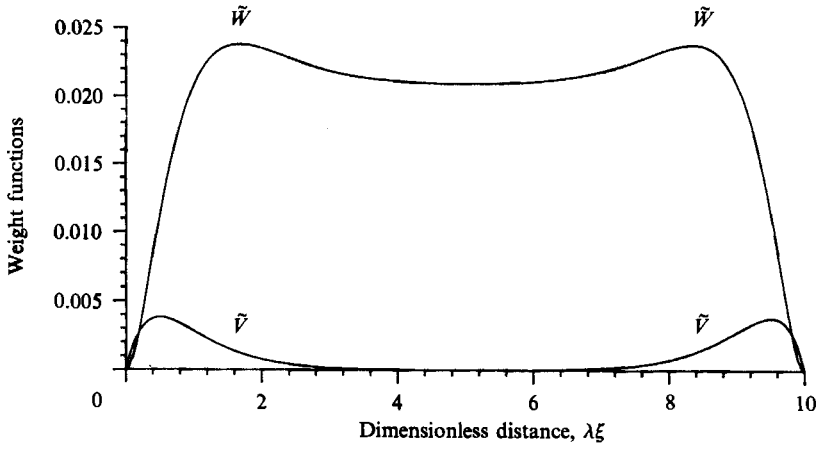

FIGURE 4. One-dimensional weight functions $\tilde{W}$ and $\tilde{V}$ for the main contribution σ^2 and end correction Δ^2 to the temporal variance.

Figure 4 shows the one-mode versions of these weight functions for the special case $\lambda^* l = 10$. As in figure 3, the $\tilde{V}$ weight function is localized to the end points. By contrast, $\tilde{W}$ is virtually constant in the central region:

$$\tilde{W} \approx \sum_{n=1}^{\infty} \frac{(\bar{\phi}_n)^2}{\lambda_n} = \frac{(\overline{\phi^*})^2}{\lambda^*} = (\tfrac{1}{48} \text{ for Poiseuille pipe flow}). \tag{11.8}$$

In terms of the conventional x-coordinate, the single integral formulae for σ^2 and Δ^2 are

$$\sigma^2(L) = 2\int_0^L \frac{a^2}{\kappa \bar{u}} \tilde{W}(x)\,\mathrm{d}x, \tag{11.9a}$$

$$\Delta^2(L) = 2\int_0^L \frac{a^2}{\kappa \bar{u}} \tilde{V}(x)\,\mathrm{d}x. \tag{11.9b}$$

In the slowly varying limit we can obtain the approximations

$$\sigma^2(L) = 2\frac{(\overline{\phi^*})^2}{\lambda^*}\int_0^L \frac{a^2}{\kappa \bar{u}}\mathrm{d}x, \tag{11.10a}$$

$$\Delta^2(L) = \frac{(\overline{\phi^*})^2}{2\lambda^{*2}}\left[\frac{a^4}{\kappa^2}\bigg|_0 + \frac{a^4}{\kappa^2}\bigg|_L\right]. \tag{11.10b}$$

The combination $\Delta^2 T^2/\sigma^4$ arose in the expression (7.5 *b*) for the response function. The formulae (7.1*a*), (11.9*a*, *b*) for the ingredients T, σ^2, Δ^2 lead to the result

$$\frac{\Delta^2 T^2}{\sigma^4} = \frac{1}{8(\overline{\phi^*})^2}\left[\frac{a^4}{\kappa^2}\bigg|_0 + \frac{a^4}{\kappa^2}\bigg|_L\right]\left(\int_0^L \frac{\mathrm{d}x}{\bar{u}}\right)^2 \Big/ \left(\int_0^L \frac{a^2\,\mathrm{d}x}{\kappa \bar{u}}\right)^2. \tag{11.11}$$

A change of scaling for the capillary radius a, transverse diffusivity κ, flow velocity $\bar{u}$, or the length L does not modify the value of this combination of terms. For example, for uniform Poiseuille pipe flow, with a, κ, $\bar{u}$ all constant, we obtain

$$\frac{\Delta^2 T^2}{\sigma^4} = \frac{3}{4}. \tag{11.12}$$

For compressible, isothermal flows with a 10:1 pressure drop, our subsequent results for T, σ^2 and Δ^2 yield

$$\frac{\Delta^2 T^2}{\sigma^4} = 0.68. \tag{11.13}$$

12. Calculating the flow

We shall regard the temperature distribution $\Theta(x)$, and hence the viscosity distribution $\mu(x)$, along the capillary as being prescribed. (This implies rapid adjustment of internal energy, which becomes invalid under 'choking' conditions.) For given entry and exit pressures P_0, P_L we seek the pressure distribution $P(x)$, and subsequently the slowness distribution $1/\bar{u}(x)$.

Cross-sectionally averaged versions of the mass, momentum and perfect gas laws are

$$\frac{\mathrm{d}}{\mathrm{d}x}(\rho a^2 \bar{u}) = 0, \quad -\frac{\mathrm{d}P}{\mathrm{d}x} = 8\frac{\mu \bar{u}}{a^2}, \quad P = R\rho\Theta, \tag{12.1a–c}$$

where R is the gas constant. For simplicity, a non-uniform advection term $\rho\overline{u\partial_x u} = \frac{4}{3}\rho\bar{u}\,\partial_x \bar{u}$ has been neglected in the momentum equation (i.e. viscous drag dominates form drag). This approximation is accurate except for Reynolds' numbers in excess of L/a (see Appendix B).

From the perfect gas law (12.1c), we can eliminate ρ in favour of P. A first integral of the mass conservation equation (12.1a) is then

$$\rho a^2 \bar{u} = \frac{P a^2 \bar{u}}{R\Theta} = F, \tag{12.2}$$

where F is a constant to be determined (a measure of the mass flow rate along the capillary). Eliminating $\bar{u}$ in favour of P, leads us to the momentum equation

$$-\frac{\mathrm{d}P}{\mathrm{d}x} = 8RF\frac{\mu\Theta}{Pa^4}. \tag{12.3}$$

To match the entry and exit pressures P_0, P_L, the flow rate constant F must have the value

$$16RF\int_0^L \frac{\mu\Theta}{a^4}\mathrm{d}x = P_0^2 - P_L^2. \tag{12.4}$$

The corresponding solution for $P(x)^2$ is

$$P(x)^2\int_0^L \frac{\mu\Theta}{a^4}\mathrm{d}x' = P_0^2\int_x^L \frac{\mu\Theta}{a^4}\mathrm{d}x' + P_L^2\int_0^x \frac{\mu\Theta}{a^4}\mathrm{d}x'. \tag{12.5}$$

Finally, the solution for the slowness can be written

$$\frac{1}{\bar{u}} = \frac{16a^2}{\Theta[P_0^2 - P_L^2]}\left\{\int_0^L \frac{\mu\Theta}{a^4}\mathrm{d}x'\right\}^{\frac{1}{2}}\left\{P_0^2\int_x^L \frac{\mu\Theta}{a^4}\mathrm{d}x' + P_L^2\int_0^x \frac{\mu\Theta}{a^4}\mathrm{d}x'\right\}^{\frac{1}{2}}. \tag{12.6}$$

For isothermal flows, with Θ and μ both constant, the solution (12.6) simplifies further:

$$\frac{1}{\bar{u}} = \frac{16\mu L}{[P_0^2 - P_L^2]}\left\{\frac{1}{L}\int_0^L \frac{\mathrm{d}x'}{a^4}\right\}^{\frac{1}{2}}\left\{P_0^2\frac{a^4}{L}\int_x^L \frac{\mathrm{d}x'}{a^4} + P_L^2\frac{a^4}{L}\int_0^x \frac{\mathrm{d}x'}{a^4}\right\}^{\frac{1}{2}}. \tag{12.7}$$

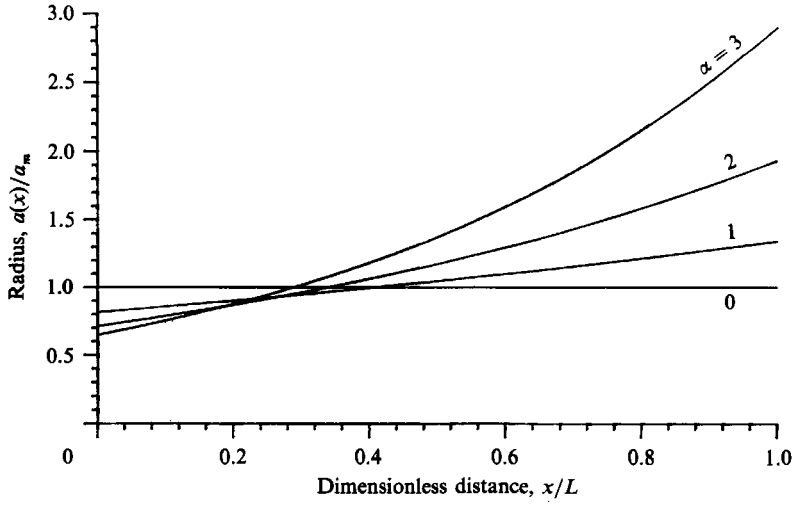

FIGURE 5. Pipe radius for different values of α. In isothermal conditions the mass flow rate is independent of α.

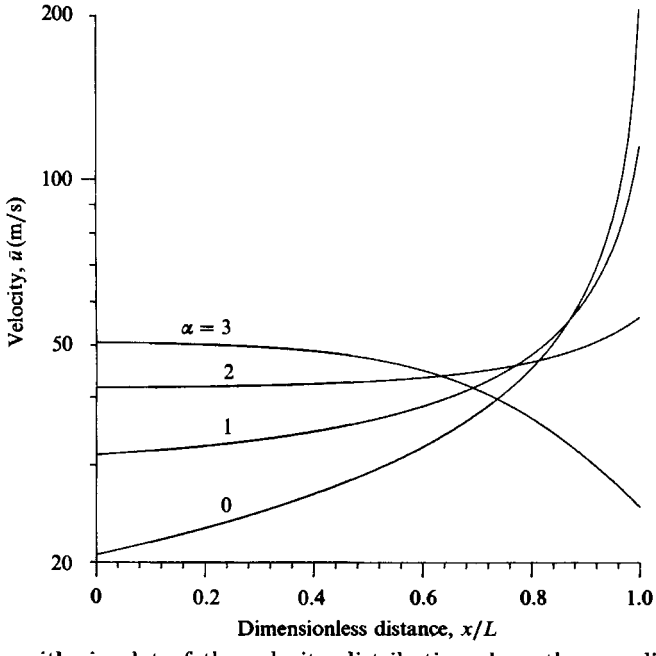

FIGURE 6. Logarithmic plot of the velocity distribution along the sampling tube for the flow specification given in (12.10). Halving the area of the capillary, or doubling the length, reduces the velocities by a factor of two.

A family of horn-shaped pipe profiles (see figure 5), for which the isothermal mass flow rate is the same, is

$$a(x) = a_m \left(\frac{\sinh \alpha}{\alpha}\right)^{\frac{1}{4}} \exp\left(\frac{\alpha x}{2L} - \frac{\alpha}{4}\right). \tag{12.8}$$

The formula (12.7) for the slowness becomes

$$\frac{1}{\bar{u}} = \frac{16\mu L}{a_m^2[P_0^2 - P_L^2]} \left\{ P_0^2 \frac{1 - \exp(2\alpha(x/L) - 2\alpha)}{2\alpha} + P_L^2 \frac{\exp(2\alpha(x/L)) - 1}{2\alpha} \right\}^{\frac{1}{2}}. \tag{12.9}$$

As a quantitative example, we specify

$$\left.\begin{aligned} P_0 &= 10 \text{ bar} = 10^6 \text{ kg m}^{-1} \text{ s}^{-2}, \\ P_L &= 1 \text{ bar} = 10^5 \text{ kg m}^{-1} \text{ s}^{-2}, \\ \mu &= 2.5 \times 10^{-5} \text{ kg m}^{-1} \text{ s}^{-1}, \\ a_m &= 0.05 \text{ mm}, \quad L = 0.3 \text{ m}. \end{aligned}\right\} \tag{12.10}$$

Figure 6 gives a logarithmic plot of the velocity distribution. In the constant-radius case ($\alpha = 0$), the Reynolds' number has the constant value 300 but the velocity ranges from 21 ms^{-1} at the high pressure entry up to 210 ms^{-1} with Mach number 0.47 at the low pressure exit. (At even higher velocities there is the possibility of 'choking'.) So, there are indeed substantial changes in flow conditions along the capillary. A noteworthy exception is when the change in flow area exactly matches the gaseous expansion:

$$\alpha = \ln (P_0/P_L). \tag{12.11}$$

In this exceptional case, the velocity is constant at 44 m s^{-1}.

The appropriateness of the single integral formula (11.5) for the temporal variance can be assessed by the straightness over a mixing length of the curves in figure 6. The estimates following equation (8.3) suggest that near the exit the mixing length is only about 6.25 mm. So, we infer that the exponentially varying approximation is indeed applicable.

In general, it is not possible to evaluate the time-of-transit integral (7.1a) explicitly. However, there are two values of α for which we can obtain explicit formulae:

$$T = \frac{32\mu L^2[P_0^3 - P_L^3]}{3a_m^2[P_0^2 - P_L^2]^2} \quad \text{for} \quad \alpha = 0, \tag{12.12a}$$

$$T = \frac{16\mu L^2}{a_m^2[P_0^2 - P_L^2]^{\frac{1}{2}}[2\ln (P_0/P_L)]^{\frac{1}{2}}} \quad \text{for} \quad \alpha = \ln (P_0/P_L). \tag{12.12b}$$

For the numerical specifications (12.10), the formula (12.12a) gives the transit time from engine to detector to be 0.0098 s. With the same mass flow rate, the horn-shaped case (12.12b) yields the transit time 0.0068 s. It is the shortness of these travel times that permits us to regard the flow conditions within the capillary as being steady, even when an internal combustion engine is being monitored. For engine speeds beyond 3000 r.p.m., account would need to be taken of the unsteadiness.

13. Evaluating the temporal variance

We model the diffusivity as being proportional to the viscosity and inversely proportional to the density (Batchelor 1967, 1.7.29–30):

$$\kappa = k\mu/\rho = kR\mu\Theta/P, \tag{13.1}$$

where k is a dimensionless constant. For nitrogen $k = 1.25$, while for the higher molecular weight constituents k will be smaller. (Our illustrative numerical examples are based upon the value $k = 0.15$, which is more representative of the hydrocarbon fuel.)

Conveniently, the integrand in (8.4) for the intrinsic coordinate ξ is proportional to $\mu(x)$:

$$\frac{\kappa}{a^2\bar{u}} = \frac{k}{F}\mu, \tag{13.2}$$

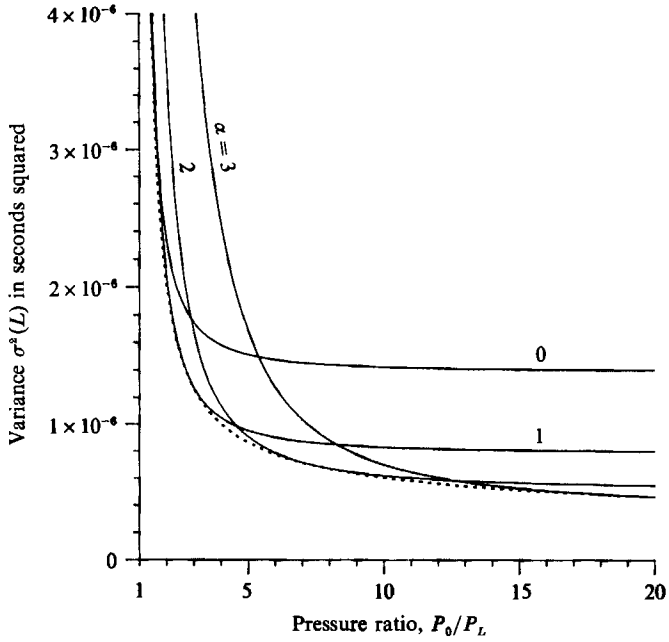

FIGURE 7. Main contribution $\sigma^2(L)$ to the temporal variance for varied pressure ratios, with the flow specification (13.6). Doubling the length L increases $\sigma^2(L)$ by a factor of four. For a lower molecular weight fuel with double the diffusivity, the temporal variance would be halved.

where the flow rate constant F is given by (12.4). Thus, in the isothermal case, with $\mu(x)$ constant, the intrinsic coordinate ξ is proportional to x. Also, the integrand required in the double integral formula (9.2) for the temporal variance is proportional to the slowness:

$$\frac{a^2}{\kappa} = \frac{F}{k\mu\bar{u}}. \tag{13.3}$$

So, in the isothermal case, an exponential variation for a^2/κ corresponds to an exponential variation for the velocity $\bar{u}$. This justifies the use in figure 6 of a logarithmic plot in order to test the applicability of the single integral formula (11.5) for $\sigma^2(L)$.

In the isothermal case with exponential pipe geometry, and laminar Poiseuille flow, the single integral formula (11.5) can be written

$$\sigma^2(L) = \frac{32L^2}{kR\Theta[P_0^2-P_L^2]}\int_0^L \tilde{W}(x)\left\{P_0^2\frac{1-\exp(2\alpha(x/L)-2\alpha)}{2\alpha}+P_L^2\frac{\exp(2\alpha(x/L))-1}{2\alpha}\right\}\mathrm{d}x. \tag{13.4}$$

It is the P_0^2 term in the integrand that strongly weights the spreading to the high-pressure end of the sampling tube. If we assume that $16l$ is large compared with $|\alpha|$, then the further approximation (11.10a) is applicable, and we obtain the explicit formula

$$\sigma^2(L) = \frac{2L^2}{3kR\Theta[P_0^2-P_L^2]}\left\{P_0^2\left[\frac{\exp(-2\alpha)-1+2\alpha}{(2\alpha)^2}\right]+P_L^2\left[\frac{\exp(2\alpha)-1-2\alpha}{(2\alpha)^2}\right]\right\}. \tag{13.5}$$

This is independent of the reference radius a_m, and scales as the square of the pipe length.

The sharpness of the response is extremely sensitive to the length L of the sampling

tube. Thus, the measuring equipment should be as close as possible to the engine (subject to the survival of the equipment). The inverse dependence of σ^2 upon the thermodynamic temperature Θ, indicates that the sampling tube should be kept as hot as possible. Heating the tube has other practical advantages such as the elimination of condensation of fuel droplets on the wall of the capillary (N. Collings 1988, personal communication). Similarly, the inverse dependence of σ^2 upon the constant k, indicates that the higher molecular weight chemical constituents are more subject to spreading. (Hence our using a value of k appropriate to fuel and not to air, in the illustrative examples.)

Figure 7 shows the temporal variance σ^2 as a function of the pressure ratio P_0/P_L for the parameter values

$$L = 0.3\text{ m}, \quad k = 0.15, \quad R = 287\text{ m}^2\text{ s}^{-1}\text{ K}^{-1}, \quad \Theta = 500\text{ K}. \tag{13.6}$$

In particular, at our standard pressure ratio of 10:1 and with constant capillary radius ($\alpha = 0$), the formula (13.5) yields the astonishingly sharp response

$$\sigma^2(L) = 1.4 \times 10^{-6}\text{ s}^2 \quad \text{with} \quad \alpha = 0. \tag{13.7}$$

This is compatible with the estimate 0.9×10^{-3} s for the response time obtained experimentally by Collings (1988, figure 3). There is a marked deterioration in the sharpness of the response at low pressure ratios. Thus, for low pressure engines it is advantageous to reduce the pressure P_L within the monitoring equipment.

For a fixed pressure ratio, the sharpest response is at

$$\alpha = \ln(P_0/P_L) \tag{13.8}$$

(i.e. the constant-velocity case). The dotted curve in figure 7 shows this optimal response. It is at low pressure (when the accuracy is worst) that a uniform radius ($\alpha = 0$) is optimal for isothermal flows. At our standard pressure ratio of 10:1 the optimal horn shape sharpens the temporal variance to

$$\sigma^2(L) = 6 \times 10^{-7}\text{ s}^2 \quad \text{with} \quad \alpha = 2.3. \tag{13.9}$$

For comparison, we record that the formula (11.10b) for the deficit variance $\Delta^2(L)$ is

$$\Delta^2(L) = \frac{a_m^4 \sinh\alpha}{1536\,\alpha k^2 R^2 \mu^2 \Theta^2}[\exp(-\alpha)P_0^2 + \exp(\alpha)P_L^2]. \tag{13.10}$$

Using the parameter values given in (12.10), (13.6), we obtain

$$\Delta^2(L) = 1.4 \times 10^{-8}\text{ s}^2 \quad \text{for} \quad \alpha = 0, \tag{13.11a}$$

$$\Delta^2(L) = 6 \times 10^{-9}\text{ s}^2 \quad \text{for} \quad \alpha = 2.3. \tag{13.11b}$$

The disparity between σ^2 and Δ^2 confirms that the sampling tube is indeed sufficiently long for the applicability of the present analysis.

14. Optimization

In the slowly varying limit (11.10a), the non-isothermal counterpart to equation (13.5) is

$$\sigma^2(L) = \frac{2}{3kR[P_0^2 - P_L^2]} \int_0^L \frac{a^4}{\mu\Theta^2} \left\{ P_0^2 \int_x^L \frac{\mu\Theta}{a^4}\,dx' + P_L^2 \int_0^x \frac{\mu\Theta}{a^4}\,dx' \right\}. \tag{14.1}$$

For fixed $\mu(x)$ and $\Theta(x)$ we can optimize for a^4. The first variation with respect to δa^4 yields the optimization condition

$$\frac{1}{\mu\Theta^2}\left\{ P_0^2 \int_x^L \frac{\mu\Theta}{a^4}\,dx' + P_L^2 \int_0^x \frac{\mu\Theta}{a^4}\,dx' \right\} = \frac{\mu\Theta}{a^8}\left\{ P_0^2 \int_0^x \frac{a^4}{\mu\Theta^2}\,dx' + P_L^2 \int_x^L \frac{a^4}{\mu\Theta^2}\,dx' \right\}. \tag{14.2}$$

The solution for a^4 is

$$a^4 = \text{constant} \times \mu \Theta^{\frac{3}{2}} \exp\left(2\alpha \int_0^x \Theta^{-\frac{1}{2}} \mathrm{d}x' \Big/ \int_0^L \Theta^{-\frac{1}{2}} \mathrm{d}x'\right), \tag{14.3a}$$

with

$$\alpha = \ln(P_0/P_L). \tag{14.3b}$$

Thus, in the isothermal case an exponential shape with the value of α given by (13.8) is optimal with respect to all possible shapes.

The minimum temporal variance is

$$\sigma^2(L) = \frac{1}{3kR \ln(P_0/P_L)} \left[\int_0^L \Theta^{-\frac{1}{2}} \mathrm{d}x\right]^2. \tag{14.4}$$

This formula shows the relative importance of the coldest part of the capillary, and hence the efficacy of heating the sampling tube.

I wish to thank George Batchelor and Nick Collings for drawing my attention to this problem. Financial support from The Royal Society is gratefully acknowledged.

Appendix A. One-mode approximation

The principal contribution σ^2 to the temporal variance will be accurately modelled provided that we can reproduce the property (9.4):

$$\int_0^l W(\xi, \xi') \mathrm{d}\xi = \sum_{n=1}^{\infty} \frac{(\bar{\phi}_n)^2}{\lambda_n}. \tag{A 1}$$

Similarly, the deficit variance Δ^2 associated with the end points will be accurately modelled if we can preserve the property (10.4):

$$\int_0^l \int_0^l V(\xi, \xi') \mathrm{d}\xi \mathrm{d}\xi' = \sum_{n=1}^{\infty} \frac{(\bar{\phi}_n)^2}{\lambda_n^2}. \tag{A 2}$$

To avoid the need to evaluate all the coefficients, $\bar{\phi}_n, \lambda_n$ we define the function

$$G^* = \sum_{n=1}^{\infty} \frac{\bar{\phi}_n}{\lambda_n} \phi_n(r) \tag{A 3}$$

(a dimensionless counterpart to the time-lag functions $G^{(+)}, G^{(-)}$).

It is easy to verify that

$$\bar{G}^* = \sum_{n=1}^{\infty} \frac{(\bar{\phi}_n)^2}{\lambda_n}, \quad \overline{\frac{u}{\bar{u}} G^{*2}} = \sum_{n=1}^{\infty} \frac{(\bar{\phi}_n)^2}{\lambda_n^2}. \tag{A 4a, b}$$

Furthermore, G^* satisfies the equations

$$\frac{1}{r} \frac{\mathrm{d}}{\mathrm{d}r}\left(r \frac{\mathrm{d}G^*}{\mathrm{d}r}\right) = \frac{u}{\bar{u}} - 1, \tag{A 5a}$$

with

$$\frac{\mathrm{d}G^*}{\mathrm{d}r} = 0 \quad \text{on} \quad r = 1, \tag{A 5b}$$

and

$$\overline{uG^*} = 0. \tag{A 5c}$$

which can be solved without involving ϕ_n or λ_n. In particular, for Poiseuille pipe flow

$$G^*(r) = \tfrac{1}{16}\{-1 + 4r^2 - 2r^4\}. \tag{A 6}$$

In terms of G^* we define the one-term approximations

$$\phi^*(r) = G^*(r) \Big/ \left(\overline{\frac{u}{\bar{u}} G^{*2}}\right)^{\frac{1}{2}}, \tag{A 7a}$$

$$\lambda^* = \overline{G^*} \Big/ \overline{\frac{u}{\bar{u}} G^{*2}}. \tag{A 7b}$$

By construction, the one-mode approximations correctly reproduce the results (A 4a, b):

$$\overline{G^*} = \frac{(\overline{\phi^*})^2}{\lambda^*}, \quad \overline{\frac{u}{\bar{u}} G^{*2}} = \frac{(\overline{\phi^*})^2}{\lambda^{*2}}. \tag{A 8a, b}$$

So, both σ^2 and Δ^2 are accurately modelled.

Appendix B. The small effect upon the flow of non-uniform advection

For the constant-radius isothermal case it is easy to investigate the role of non-uniform advection in the momentum equation:

$$-\frac{\mathrm{d}P}{\mathrm{d}x} = \frac{8\mu\bar{u}}{a^2} + \tfrac{4}{3}\rho\bar{u}\,\partial_x \bar{u}. \tag{B 1}$$

As in §12, we use the perfect gas law to eliminate ρ in favour of P, and the conservation of mass flux F to eliminate $\bar{u}$:

$$-\frac{\mathrm{d}P}{\mathrm{d}x} = \frac{8\mu F R\Theta}{a^4 P} - \frac{4F^2 R\Theta}{3a^4 P^2}\frac{\mathrm{d}P}{\mathrm{d}x}. \tag{B 2}$$

This equation can be integrated to give an implicit formula for $P(x)$:

$$P(x)^2 - P_L^2 = \frac{16\mu F R\Theta}{a^4}(L-x) + \frac{8F^2 R\Theta}{3a^4}\ln\left(P(x)/P_L\right). \tag{B 3}$$

Hence, the non-uniform advection is associated with the logarithmic term.

Matching with the engine pressure P_0 at $x = 0$ yields a quadratic equation for the mass flux F. We can write the solution for F as a perturbation about the linear solution:

$$F = \frac{a^4}{8R\mu\Theta L}\frac{P_0^2 - P_L^2}{1+(1+\epsilon)^{\frac{1}{2}}}, \tag{B 4}$$

where

$$\epsilon = \frac{a^4[P_0^2 - P_L^2]\ln\left(P_0/P_L\right)}{96\mu^2 R\Theta L^2}. \tag{B 5}$$

For small ϵ the error associated with the neglect of non-uniform advection is of order $\frac{1}{4}\epsilon$.

To estimate ϵ we can use the simplified solutions given in §12. For a constant-radius, isothermal flow the Reynolds number is constant

$$Re = \frac{\rho\bar{u}a}{\mu} = \frac{F}{a\mu} \sim \frac{a^3}{16\mu^2 R\Theta L}[P_0^2 - P_L^2]. \tag{B 6}$$

Hence, we arrive at the estimate

$$\epsilon = \frac{aRe}{6L}\ln\left(P_0/P_L\right). \tag{B 7}$$

So, for $\frac{1}{4}\epsilon$ to be small, and for non-uniform advection to be unimportant, it suffices that the Reynolds number is less than L/a (typically 6000). This is well satisfied for the examples considered in the above paper.

REFERENCES

BATCHELOR, G. K. 1967 *An Introduction to Fluid Dynamics*. Cambridge University Press.

CARSLAW, H. S. & JAEGER, J. C. 1959 *Conduction of Heat in Solids*. Oxford University Press.

COLLINGS, N. 1988 A new technique for measuring HC concentration in real time, in a running engine. *SAE* 880517.

ERDOGAN, M. E. & CHATWIN, P. C. 1967 The effect of curvature and buoyancy on the laminar dispersion of solute in a horizontal tube. *J. Fluid Mech.* **29**, 465–484.

JOHNSON, S. C. 1979 Precombustion fuel/air distribution in a stratified charge engine using laser Raman spectroscopy. *SAE* 790433.

PHILIP, J. R. 1963*a* The theory of dispersal during laminar flow in tubes. I. *Austral. J. Phys.* **16**, 287–299.

PHILIP, J. R. 1963*b* The theory of dispersal during laminar flow in tubes. II. *Austral. J. Phys.* **16**, 300–319.

PHILIP, J. R. 1963*c* The damping of a fluctuating concentration by continuous sampling through a tube. *Austral. J. Phys.* **16**, 454–463.

RHINES, P. B. & YOUNG, W. R. 1983 How rapidly is a passive scalar mixed within closed streamlines? *J. Fluid Mech.* **133**, 133–145.

SMITH, R. 1983 Longitudinal dispersion coefficients for varying channels. *J. Fluid Mech.* **130**, 299–314.

SMITH, R. 1984 Temporal moments at large distances downstream of contaminant releases in rivers. *J. Fluid Mech.* **140**, 153–174.

TAYLOR, G. I. 1953 Dispersion of soluble matter in solvent flowing slowly through a tube. *Proc. R. Soc. Lond.* A **219**, 186–203.

TSAI, Y. H. & HOLLEY, E. R. 1978 Temporal moments for longitudinal dispersion. *J. Hydraul. Div. ASCE* **104**, 1617–1634.

TSAI, Y. H. & HOLLEY, E. R. 1980 Temporal moments for longitudinal dispersion. *J. Hydraul. Div. ASCE* **106**, 2063–2066.